造粒粒子とナノ粒子含有インクを用いたセラミックス三次元造形

Ceramics Additive Manufacturing by Granulated Particle and Nanoparticle Containing Ink

鴨田　紀一[*]　森永　匡彦[*]　萩原　弘規[**]　小西　鷹介[*]　寺井　希[**]
Kiich KAMODA　Tadahiko MORINAGA　Hiroki HAGIWARA　Yosuke KONISHI　Nozomi TERAI

早川　翔太[***]　孫　允晟[***]
Shouta HAYAKAWA　Insei SON

要　旨

セラミックスの三次元造形（Additive Manufacturing）は，構造部品の製造において従来の成形方法よりも効果的であるが，1 cm以上の厚い部品を製造する場合に割れや変形を生じやすいという問題があるため，治具やタービン部品などのエンジニアリングセラミックス部品としての適用の障壁となっている．本研究では，構造用セラミックス部品の製造に向けた新しいバインダージェッティング（BJ）方法である「粒子均質化モデリング（PHM）」を提案する．PHM法は，微量の樹脂とセラミックス一次粒子からなるセラミック造粒粉末と，セラミックナノ粒子と造粒粒子を崩壊させる溶媒を含むインクを特徴としている．本研究では，インクの飽和度の関数としてグリーン体の相対密度を評価し，提案するPHM法の効果を検証した．飽和度の増加により均質化が生じ，焼結体の最高相対密度は88 vol.%であった．さらに，厚さ10 mmから30 mmのグリーン体を焼結する場合の収縮率は一定であり，割れや変形は確認されなかった．10 mm以上の部品を変形やクラックなしに製造することは，既存研究と比較して画期的な進歩である．PHM法は，大型の高密度・高精度セラミック部品を製造する手段として有望なアプローチであり，将来さまざまな産業分野への応用が期待できる．

ABSTRACT

Ceramic additive manufacturing is generally more effective than conventional molding methods when used for structural parts, but the modeling quality (e.g., accuracy, density) is limited when manufacturing thick parts. In particular, engineering ceramic parts such as a jig or turbine components are 1 to several centimeters thick. This study presents a novel binder jetting (BJ) method called particle homogenizing modeling (PHM) for manufacturing structural ceramics. The PHM method is characterized by the ceramic granulated particles used for the recoating powder, and ink which contains ceramic nanoparticles and a solvent that collapses the granulated particles. In this study, the relative density of the green body is evaluated as a function of the ink saturation to verify the effectiveness of the proposed PHM method. Homogenization occurs due to increased saturation, and consequently, the highest value of the relative density of the sintered body is 88 vol.%. Furthermore, less deformation or cracking is observed when compared to previous studies, and the shrinkage rate is constant when green bodies with a thickness of 10 mm to 30 mm are sintered. Building parts 10 mm or thicker without deformation or cracking would be a groundbreaking advancement in the ceramics additive manufacturing field. The novel PHM method can potentially be used to manufacture large, high-density, high-precision ceramic parts, and can also be applied in various industrial fields in the future.

*　先端技術研究所　IDPS研究センター
Industrial Digital Printing System Institute, Advanced technology R&D Division
**　リコーフューチャーズBU　IJ電池事業センター　副業で参加
IJ Printed Battery Solution Business Center, Ricoh Futures BU
***　リコーフューチャーズBU　AM事業センター　副業で参加
Additive Manufacturing Business Center, Ricoh Futures BU

1. Introduction

1-1 Background

Advanced ceramic materials (e.g., alumina, zirconia, and silicon carbide) are applied as structural materials such as engine components in the aerospace, automotive, and heavy electrical industries to reduce the environmental impact owing to their excellent material properties such as mechanical strength, low weight, high melting point, and resistance to environmental factors[1].

However, the conventional manufacturing methods used to process ceramics into structural parts are time-consuming and expensive. Furthermore, these methods are generally incompatible when used for parts with complicated shapes and high thickness. Machining is one of the conventional methods of ceramic processing. It can be used to manufacture large and thick ceramic parts from sintered blocks. However, it is disadvantageous as cracks or fractures tend to develop when processing thin or small parts. The ceramic injection molding (CIM) method is another widely used conventional method for ceramic processing[2-5]. In this method, a binder and solvent are added to the ceramic powder and kneaded to produce a ceramic paste, which is molded with an extrusion molding machine. Subsequently, the molded body (green body) is generally subjected to heat treatment to remove the mixed resin (debinding process) and sintered at a high temperature. The CIM method is suitable for processing small or thin parts, but not for machining thick parts because the paste and green body have many impurities to ensure good flowability or handling. Consequently, deformation and cracking tend to occur during the debinding process for thick or large parts[2-5]. Many engineering ceramics parts like jig and turbine components have a thickness from 1~few centimeters.

Additive manufacturing (AM) can be used to overcome these problems and presents considerable potential as an effective approach for manufacturing structural ceramic parts[6-9]. Several methods have been proposed for the manufacturing of three-dimensional ceramics[8,9], binder jetting (BJ), vat photopolymerization (VP), powder bed fusion (PBF), directed energy deposition (DED), material extrusion (ME), material jetting (MJ), and sheet lamination (SL). Each AM method presents various advantages and disadvantages in the manufacturing of structural ceramics. The VP and MJ methods can be used to produce parts with excellent accuracy, high density, and good surface roughness as these methods involve the use of nanoscale ceramic particles in the raw materials. However, these methods are limited by the thickness of the parts, similar to the CIM method[10-12]. The VP method uses a ceramic paste containing a large amount of resin in the raw material. The MJ method uses ceramic particles which contain ink and use many resins as solidifying agents. Deformation, cracking, pores, and residual carbon are generated during the debinding and sintering process for thick or large parts since resin is an impurity[10, 13, 14]. In contrast, the BJ method can be used to manufacture parts using lower amounts of resin when compared to the other methods[7,15-18]. The BJ process uses a binder to stick the powders and the amount of binder to be discharged is minimal since the powder occupies the majority volume in parts. However, the BJ method is also disadvantageous as it is difficult to achieve both high density and high accuracy. Powder flowability and packing density are important parameters in evaluating materials in the powder bed method for the quality of the parts, such as density, accuracy, surface roughness, and so on[16]. These powder parameters correspond intricately to various properties, such as particle size, and roundness. Consequently, materials with a particle size of 10–50 μm are primarily used as the BJ materials[7]. Conversely, a smaller particle size is preferable for producing dense ceramics parts such as a nanoparticle from the perspective of sinterability. However, nanoparticles are extremely difficult to handle when using the powder bed method owing to their low flowability. Therefore, forming a dense

green body with a small amount of resin component is crucial while using small particles in order to obtain thick and large ceramic sintered bodies which can be employed as a structural part.

This study proposes a novel BJ method called the particle homogenizing modeling (PHM) for manufacturing structural ceramics using smaller-sized particles, which cannot be handled by the conventional powder bed method, by using granulated particles and ceramic particle dispersion ink to overcome the existing limitations.

1-2 Particle Homogenizing Modeling

Fig. 1 illustrates the concept of the PHM method used in this study. In this process, a recoating roller is used to spread a powder layer using the granulated particles (GP) containing the primary ceramic particles (PP) and the binder resin. Subsequently, the ink is applied to the powder layer, which contains dispersed ceramic nanoparticles (DP) and the solvent, which can dissolve the binder resin in the GP. The ink, which is applied to the powder using an inkjet system, percolates into the powder by dissolving the resin contained within the granulated particles. The force binding the primary particles gradually decreases as the resin dissolves, and the granulated particles break apart from the primary particles when a certain threshold is exceeded.

Consequently, the region to which the liquid is applied, is homogenized through the shape disintegration of the secondary particles and immobilized by the binder resin, thus ensuring the reduction of voids or unsolidified regions from the region to which the liquid is applied. Furthermore, the ink contains ceramic nanoparticles to suppress the deformation which occurs during homogenization and while filling the voids. The formation and application steps are repeated until the required number of laminated layers are achieved. Miao et. al[19], Hotta et. al.[20], and Huang et. al.[21] proposed an application of the BJ method using GP to improve the handleability of fine powders, and Zhao et. al.[22] reported a method using nanoparticle ejection filled powder voids and improved the hydration resistance of 3D printed parts. However, there have been no studies conducted on a method to dissolve a granulating binder with ink and fill voids with nanoparticles in the ink.

This report describes the basic behavior of the PHM method which the effects of the amount of ink and nanoparticles applied to the granulated particles are evaluated and effect of homogenization.

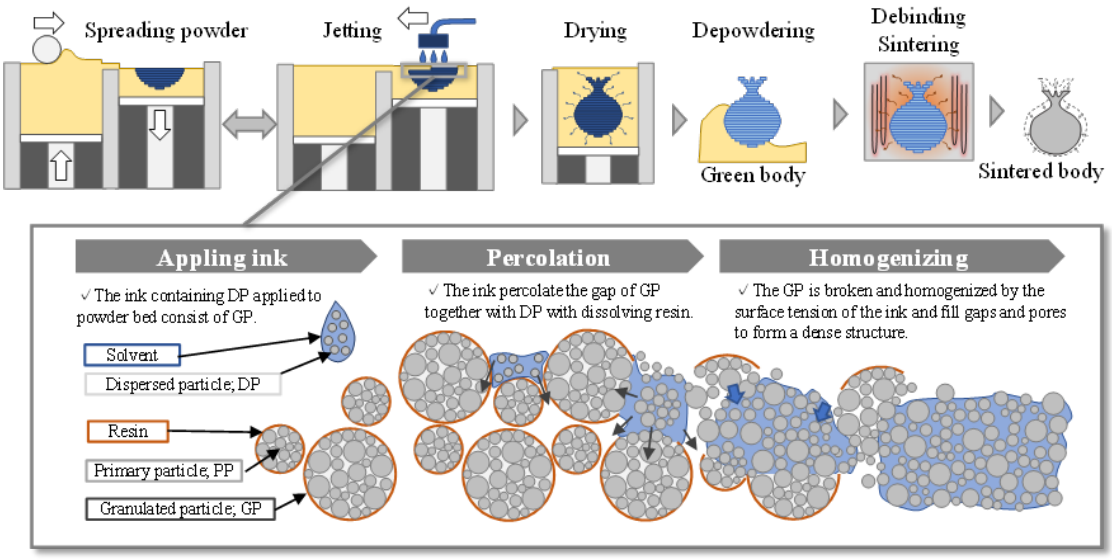

Fig. 1 Schematic illustration of particle homogenizing modeling (PHM) process.

2. Experimental

2-1 Materials

The target material used is Al_2O_3, whose effects can be easily verified by the large amount of experimental data that have been reported. The Al_2O_3 particle prepared by our research team has a purity of 99.99% and density of 3.95 g/cm^3. The Al_2O_3 particles with a volume median particle size of few microns are as the primary particle (PP), while <10 wt.% of acrylic resin is used as the binder for the granulated particles (GP). They are both mixed and dispersed with ZrO_2 beads to prepare a slurry, which is then granulated into a spray granulator. The Al_2O_3 nanoparticles with a purity of 99.99% are used for dispersed particles (DP) in ink. The difference in the particle size between the GP and DP helps in distinguishing between them to ensure that the phenomenon can be accurately understood. The DP is dispersed by a ball mill in a solvent which dissolve acrylic resin by with a dispersant for 6 h using ZrO_2 beads. The DP content is adjusted to ensure that the viscosity can be discharged using the inkjet head.

2-2 Printing process

The test pieces are fabricated using a self-developed 3D printer, which uses RICOH MH5420 as the inkjet head. The roller movement speed and roller rotation speed are 100 mm/s and 240 rpm, respectively. The layer thickness (l) is 80 μm and the ink-dripping resolution is fixed at 600 dpi. The relative ink saturation (S) is the volume fraction rate that fills volumes other than powder, with ink in the unit volume that is enveloped by ink drawing dots and layer pitch[23], and can be calculated by using the following equation:

$$Saturation, S\ [\%] = \frac{V_{ink} \times n}{(1 - \rho_P^r) \times A \times l} \qquad (1)$$

where V_{ink} represents the volume of ink per droplet ejected by the print head, n denotes the number of repeated drawings for each layer, and ρ_P^r is the relative powder bed density packed by spreading using only the roller and A represent unit area surrounded by ink dots defined by dpi. The layering process is repeated until the desired sample height is achieved. The ρ_P^r value is measured at 27 vol.%. Here, S is modeled by adjusting the discharge waveform and the number of discharges between 23.3% and 61.1%. Nine block shapes with dimensions of x:10 × y:30 × z:6 mm are built for each condition as the test pieces. X-direction is the scanning and recoating direction.

2-3 Drying, debinding, and sintering process

The part bed containing the built bodies surrounding the powder is kept in an oven for 6 h to dry following the completion of printing. The surrounding powder was removed after the drying process, and the parts are removed as a green body. The green body is heat-treated under the conditions listed in Table 1 to obtain a sintered body.

Table 1 Debinding and Sintering conditions.

Parameter	Debinding	Sintering
Temperature, Hold time	500°C, 1.5 h	1650°C, 1 h or 1700°C, 3 h
Heating rate	10°C/min	10°C/min
Cooling rate	As is	>1000°C: 5°C/min <1000°C: As is
Atmosphere	Air	Air

2-4 Characterization and measurement

The green body density (ρ_{G} g/cm^3) is calculated based on volume measured by length measurement and weight of parts since the green body includes open pores[16]. The relative density of the green body (ρ_{G}^r %) is calculated by using the following equation:

$$\rho_{\mathrm{G}}^r = \rho_{\mathrm{G}} / \rho_{\mathrm{G}}^a \qquad (2)$$

The weight ratio of the resin component of the green body is measured using Thermogravimetry-Differential

Thermal Analysis (TG-DTA), and the apparent true density (ρ_{G}^{a} g/cm^3) is obtained from the abundance ratio of the resin and alumina. The actual densities used to determine ρ_{G}^{a} are 1.2 g/cm^3 for acrylic resin and 3.95 g/cm^3 for Al_2O_3. The structural images of the green bodies and sintering bodies are observed through a scanning electron microscope (SEM; Sigma300, Carl Zeiss, Germany).

3. Result and Discussion

3-1 Green body densification behavior

Fig. 2 illustrates the correlation between the relative density of the green body and the saturation, *S*. The error bars indicate the standard deviations of the nine test pieces fabricated under similar conditions. It can be observed from Fig. 2, that the density increases with the increase in *S*. Furthermore, it can be observed that the density increase behavior has two inflection points corresponding to *S*. The dotted line represents the calculated density of the green parts based on mass balance using the following equation:

$$\rho_{\mathrm{G}}^{r} = \rho_{\mathrm{P}}^{r} + V_{\mathrm{np}} \qquad (3)$$

Here, V_{np} can be calculated from the nanoparticle content in the ink and the amount of ink dropped per voxel. This line shows a simple mass balance model of nanoparticle jetting to the powder. In Fig. 2, the plots at *S* < 35% are close to the mass balance model.

However, at 35% < *S*, the density increases significantly above the predicted mass balance model. From *S* = 35%–48%, the gradient of the density increases corresponding to the amount of ink and is more than twice that of the mass balance model. Furthermore, at *S* > 48%, the gradient becomes gentle and close to the calculated line. This shape of the curve indicates that the densification mechanism varies with an increase in the ink.

Figs. 3 (A)–(D) present the SEM images of four green body cross sections as an example. The fracture surface is formed by the 3-point bending test and the Z-direction

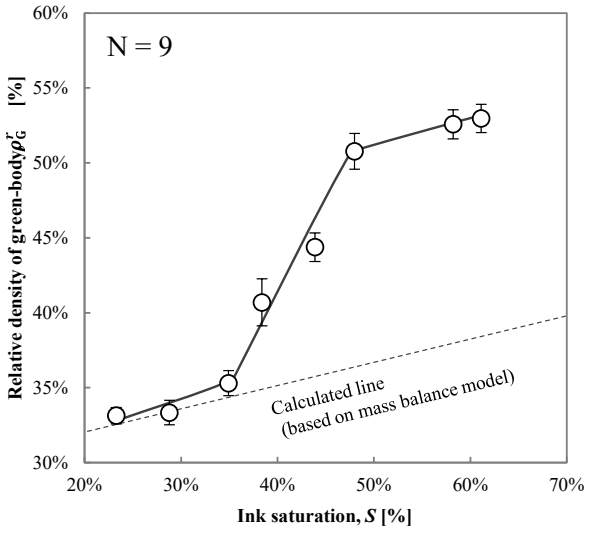

Fig. 2 The relative density of green body as a function of saturation.

indicates the upper side of the specimen. Additionally, Figs. 3 (B-1) and (B-2) present the enlarged views of (B). Three types of structures are observed at the cross section of the green bodies from the (A) to (D) images: a sparse structure in which the GP shape exists, and the DP exists on the boundary between the GPs, a homogenized structure in which the PP and DP are packed densely, and pores. In (A), which is a green body with *S* = 28.8%, ρ_{G}^{r} = 33.3%, and has a uniformly sparse structure, the shape of the GP can be confirmed on the entire surface. The sparse and homogenized structures coexist alternately with the increase in the amount of ink, as shown in (B), with *S* = 38.4% and ρ_{G}^{r} =40.7%. The shape of the GP can be identified in the sparse structure, as shown in (B-1), and it can be observed that the DP exists on the surface of the GP or between the particles. It is observed from the comparison with the shape of the GP in Fig. 1, that the resin of the GP surface can be dissolved by the ink, but the granulated shape remains unbroken. Conversely, the shape of GP in the homogenized structure and the structure in which the PP and DP are densely packed, cannot be confirmed to consist of a fracture surface, as shown in (B-2). Based on the sparse packing situation

shown in (A), it is inferred that mass transfer accompanied by large deformations is necessary to form such a dense structure. These sparse and homogenized structures alternate, and the existence of large pores with a thickness of several hundred micrometers between them, is observed. The formation of these pores can be attributed to such large deformations. Subsequently, in (C) with S = 48.0% and ρ_{G}^{r} = 50.8%, the sparse structure described above could not be confirmed, and it is composed only of pores and a homogenized structure. It can be observed from (D) that S = 61.1% and ρ_{G}^{r} = 53.0%, and that the size of the pores decreases with the increase in the amount of ink. Multiple pores with a diameter of approximately 200 μm are observed in the cross section of (D). Following the sintering process, these pores are expected to affect the strength of the parts.

The pores that can be observed in (A)–(D) are covered with smooth surfaces. It is supposed that the three-dimensional deformation is attributed to the bubbles generated through homogenization which could not

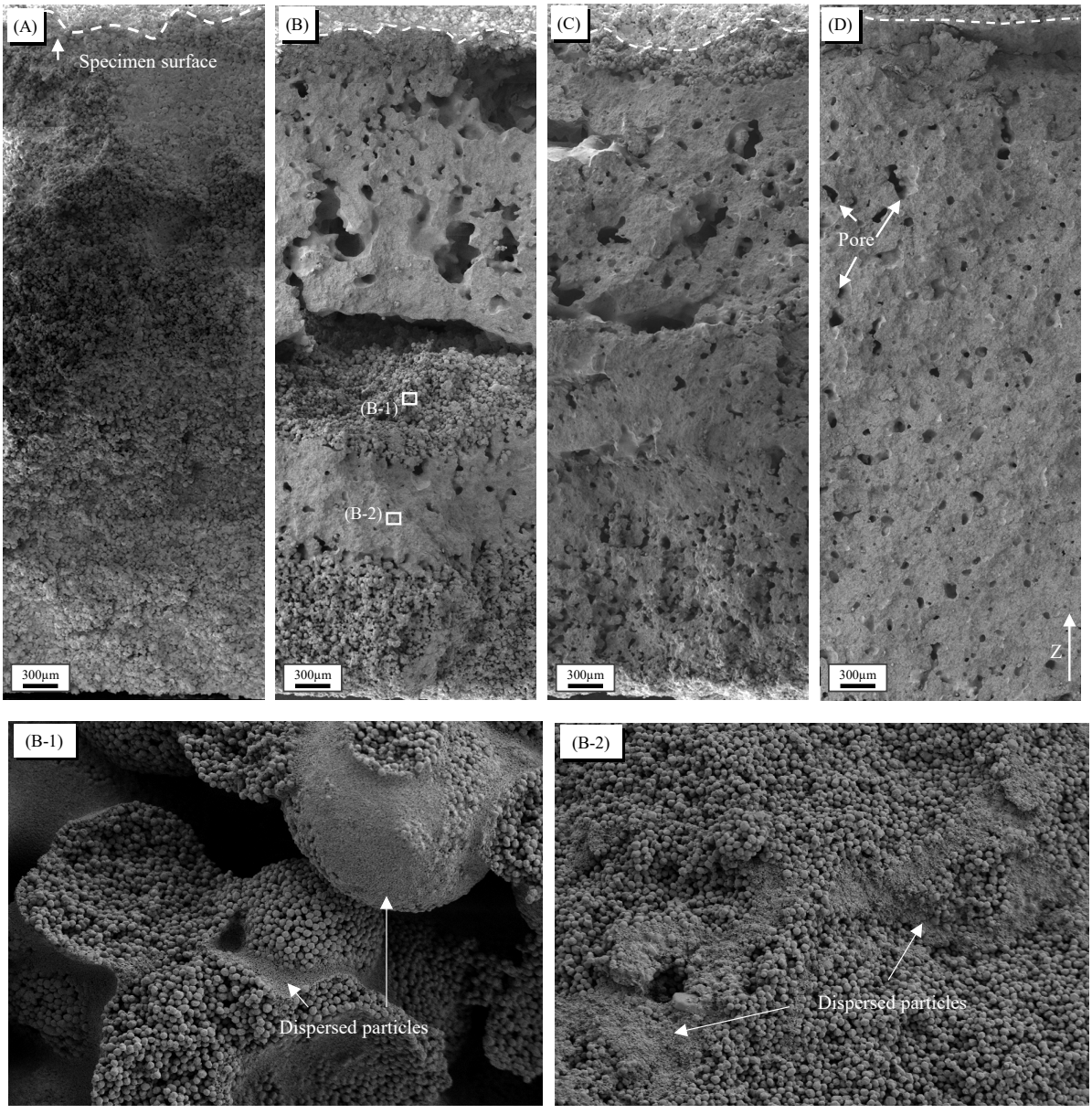

Fig. 3 SEM images of fractured surfaces of green body built at (A) S = 28.8%, ρ_{G}^{r} = 33.3%, (B) S = 38.4%, ρ_{G}^{r} = 40.7%, (C) S = 48.0%, ρ_{G}^{r} = 50.8%, and (D) S = 61.1%, ρ_{G}^{r} = 53.0%. (B-1) and (B-2) are magnified SEM images of (B).

escape due to the generation of the pores; the bubbles become voids and exist within in the green body. It can be observed from (C) to (D) that the size of pores decreases with the increase in the amount of ink, and it is expected that the DP in the ink suppresses the generation of voids or fills the voids. However, a detailed analysis of this phenomenon is required in the future.

We consider the PHM can be attributed to the presence of phenomena such as the balance and dissolution rate of the amount of solvent component in the ink and the amount of resin in the GP, the physics of the solution after resin dissolution, and the diffusion of the DP. Therefore, the quality of the modeled object can be improved by analyzing the material prescription which optimizes these phenomena.

3-2 Evaluation for the sintered body

Fig. 4 presents the relative densities before and after sintering. The plots for the sintering condition of 1650°C for 1 h in the air exhibit a good linear correlation between ρ_S^r and ρ_G^r. When a part of the test piece prepared under the condition of S = 61.1% is sintered at 1700°C for 6 h, the density is improved by 2%–8% when compared to that sintered at 1650°C for 1h. The highest density of the sintered body is ρ_S^r = 88%. It can be inferred from this linear relationship that producing a higher-density green body to realize a higher sintering density is the most effective approach.

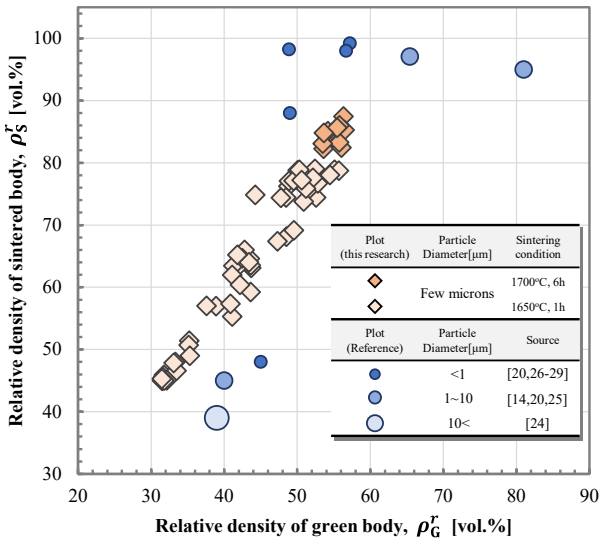

Fig. 4 The relative density of sintered body as a function of relative density of green body with reference plots.

The Al_2O_3 three-dimensional model data reported thus far are described by spherical plots as a reference for the further consideration of the effect of the PHM. The particle size is classified into three categories and is then plotted to consider the effect of the particle size of the raw material on sinterability. Hamano et al.[24] reported that a green body density of 39%, which is fabricated from 13 μm Al_2O_3 particles and has the largest particle size, exhibits almost no improvement in the density even after sintering. Azarmi et al.[14] and Zhang et al.[25] reported a sintering density of 90% or more using a particle size of 1–10 μm. They were able to produce a higher ρ_G^r using particles of similar size used in this study. The plot with a ρ_G^r of 65%[25] is an extension of the linear relationship of the plot obtained in this study. The data supports the possibility of obtaining a sintered body with a filling density close to 100% due to the improvement presented by this study. Additionally, most of the structural parts with particle sizes smaller than 1 μm have a sintering density close to 100%, even if the ρ_G^r is similar to that of this study[26-29].

Conversely, Hotta et al.[20] and Huang et al.[21] reported that there was no progress in sintering when compared to this study even though particles with a small size of 0.5 μm and 1 μm were used as raw materials. They used granulated particles in these tests to improve the powder flowability to avoid using a solvent that could collapse the granulated structure. The density is lower than that in this study due to the progress in the sintering of the PP in the GP. However, the progress in the sintering between the GP is minimal due to the large curvature between the GPs and the sintering process is limited. Therefore, the effect of homogenization in the PHM also improves the sintering density.

3-3 Hypothesis verification of PHM

The stability of the shape when a thick part is fabricated is evaluated to determine the effectiveness of the PHM method. The PHM method aims to reduce the amount of binder used when compared to other three-dimensional modeling methods proposed in the previous studies, so that a test piece with a thickness in the order of centimeters can be molded with high precision. A cube with a side length of 10–30 mm is fabricated, and the uniformity of the shrinkage rate and the stability of the relative density associated with sintering are evaluated to determine the effectiveness of the proposed method. This result is a significant advance since 6 mm thickness has been reported as critical for existing ceramics AM[10]. The modeling conditions for this model include S = 61.1%. The sintering conditions are 1650°C for 1 h. Fig. 5 presents the measurement results. The plots of the X-, Y-, and Z-axis dimensions are slightly offset to the left and right for visualization. The linearity of the edge of the sintered body of the modeled object can be confirmed. Furthermore, the dimensions of XYZ are measured at three points regardless of the size, and there is almost no variation as observed from the length measurement result presented in Fig. 5. This plot exhibits a good linear relationship, demonstrating that shrinkage due to sintering occurs uniformly regardless of the thickness of the model. Additionally, the relative densities of the green body and the sintered body are observed to be almost constant regardless of the model dimensions based on the change in the density data shown in the sphere plot, which also supports this consideration. Zhou et al.[13] reported that cracks occur when a thick test piece is molded due to the volatilization of resin components. However, in this study, cracks and deformation did not occur during debinding and sintering.

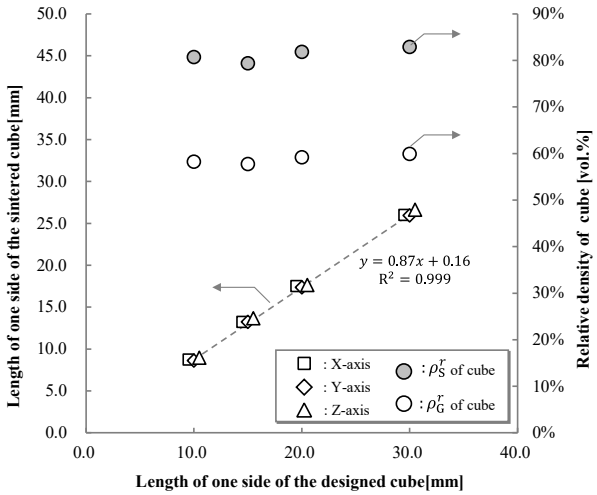

Fig. 5 Shrinkage and density stability due to sintering for cubes of different sizes.

4. Conclusion

This study proposes the particle homogenizing modeling (PHM) method to create high-density three-dimensional ceramic parts with a thickness greater than that achieved by conventional AM and reported basic behavior of this method. Fig. 6 is an example of a part built using this process. The PHM method is a type of binder jetting process which breaks the granulated powder with ink and arranges nanoparticles between the particles. The effect of ink on the behavior of densification and the variation in the internal structure was verified, and the modeling quality was evaluated. We suppose PHM would be a breakthrough in various fields where the application of ceramics is required in the future.

Fig. 6 Al_2O_3 3D printed parts built by particle homogenizing modeling (PHM) process.

References

1) M. Bengisu: Engineering ceramics, Springer Science & Business Media (2013).
2) M. Trunec, J. Cihlář: Thermal debinding of injection moulded ceramics, *J. Eur. Ceram. Soc*, Vol. 17, No. 2-3, pp. 203-209 (1997).
3) P. Thomas-Vielma et. al.: Production of alumina parts by powder injection molding with a binder system based on high density polyethylene, *J. Eur. Ceram. Soc*, Vol. 28, No. 4, pp. 763-771 (2008).
4) S. M. Ani, et. al.: Binder removal via a two-stage debinding process for ceramic injection molding parts, *Ceram. Int.*, Vol. 40, No. 2, pp. 2819-2824 (2014).
5) T. S. Shivashankar, R. M. German: Effective Length Scale for Predicting Solvent-Debinding Times of Components Produced by Powder Injection Molding, *J. Am. Ceram. Soc.*, Vol. 82, No. 5, pp. 1146-1152 (1999).
6) Z. Chen, et. al.: 3D printing of ceramics: A review, *J. Eur. Ceram. Soc.*, Vol. 39, No. 4, pp. 661-687 (2019).
7) X. Lv, et. al.: Binder jetting of ceramics: Powders, binders, printing parameters, equipment, and post-treatment, *Ceram. Int.*, Vol. 45, No. 10, pp. 12609-12624 (2019).
8) A. Zocca, et. al.: Additive Manufacturing of Ceramics: Issues, Potentialities, and Opportunities, *J. Am. Ceram. Soc.*, Vol. 98, No. 7, pp. 1983-2001 (2015).
9) A. J. Allen, I. Levin, S. E. Witt: Materials research & measurement needs for ceramics additive manufacturing, *J. Am. Ceram. Soc.*, Vol. 103, No. 11, pp. 6055-6069 (2020).
10) M. R. O'Masta, et. al.: Additive manufacturing of polymer-derived ceramic matrix composites, *J. Am. Ceram. Soc.*, Vol. 103, No. 12, pp. 6712-6723 (2020).
11) M. Pfaffinger, et. al.: Thermal Debinding of Ceramic-Filled Photopolymers, *Mater. Sci. Forum.,* Vol. 825-826, pp. 75-81 (2015).
12) S. A. Uhland, et. al.: Strength of Green Ceramics with Low Binder Content, *J. Am. Ceram. Soc.*, Vol. 84, No. 12, pp. 2809-2818 (2001).
13) M. Zhou, et. al.: Preparation of a defect-free alumina cutting tool via additive manufacturing based on stereolithography – Optimization of the drying and debinding processes, *Ceram. Int.*, Vol. 42, No. 10, pp. 11598-11602 (2016).
14) F. Azarmi, A. Amiri: Microstructural evolution during fabrication of alumina via laser stereolithography technique, *Ceram. Int.*, Vol. 45, No. 1, pp. 271-278 (2019).
15) J. Moon, et. al.: Ink-Jet Printing of Binders for Ceramic Components, *J. Am. Ceram. Soc.*, Vol. 85, No. 4, pp. 755-762 (2002).
16) W. Du, et. al.: Ceramic Binder Jetting Additive Manufacturing: A Literature Review on Density, *J. Manuf. Sci. Eng.*, Vol. 142, No. 4, p. 040801 (2020).
17) R. Melcher, et. al.: Fabrication of Al2O3-based composites by indirect 3D-printing, *Mater. Lett.*, Vol. 60, No. 4, pp. 572-575 (2006).
18) E. M. Jimenez, et. al.: Parametric analysis to quantify process input influence on the printed densities of binder jetted alumina ceramics, *Addit. Manuf.*, Vol. 30, p. 100864 (2019).
19) G. Miao, et. al.: Ceramic binder jetting additive manufacturing: Effects of granulation on properties of feedstock powder and printed and sintered parts, *Addit. Manuf.*, Vol. 36, p. 101542 (2020).
20) M. Hotta, et. al.: Powder layer manufacturing of alumina ceramics using water spray bonding, *J. Ceram. Soc. JAPAN*, Vol. 124, No. 6, pp. 750-752 (2016).
21) S. Huang, et. al.: Additive manufacturing of thin alumina ceramic cores using binder-jetting, *Addit. Manuf.*, Vol. 29, p. 100802 (2019).

22) H. Zhao, et. al.: 3D printing of CaO-based ceramic core using nanozirconia suspension as a binder, *J. Euro. Ceram. Soc.*, Vol. 37, No. 15, pp. 5119-5125 (2017).
23) A. Zocca, et. al.: LAS glass–ceramic scaffolds by three-dimensional printing, *J. Euro. Ceram. Soc.*, Vol. 33, No. 9, pp. 1525-1533 (2013).
24) R. Hamano, T. Ikoma: Preparation of α-alumina powder and binder for 3D printer, *MRS Adv.*, Vol. 3, pp. 969-975 (2018).
25) Y. Zhang, et. al.: Al2O3 Ceramics Preparation by LOM (Laminated Object Manufacturing), *Int J Adv Manuf Technol.*, Vol. 17, pp. 531-534 (2001).
26) A. Zocca, P. Lima, J. Günster: LSD-based 3D printing of alumina ceramics, *J. Ceram. Sci. Tech.*, Vol. 8, No. 1, pp. 141-148 (2017).
27) S. Mamatha, et. al.: 3D printing of complex shaped alumina parts, *Ceram. Int.*, Vol. 44, No. 16, pp. 19278-19281 (2018).
28) H. H. Tang, M. L. Chiu, H. C. Yen: Slurry-based selective laser sintering of polymer-coated ceramic powders to fabricate high strength alumina parts, *J. Eur. Ceram. Soc.*, Vol. 31, No. 8, pp. 1383-1388 (2011).
29) Z. H. Liu, et. al.: Selective Laser Sintering of High-density Alumina Ceramic Parts, *Proceedings of the 35th International MATADOR Conference* (2007).